Single-Molecule Electronics

International Edition: DOI: 10.1002/anie.201909461
German Edition: DOI: 10.1002/ange.201909461

Turning the Tap: Conformational Control of Quantum Interference to Modulate Single-Molecule Conductance

Feng Jiang, Douglas I. Trupp, Norah Algethami, Haining Zheng, Wenxiang He, Afaf Alqorashi, Chenxu Zhu, Chun Tang, Ruihao Li, Junyang Liu, Hatef Sadeghi, Jia Shi, Ross Davidson, Marcus Korb, Alexandre N. Sobolev, Masnun Naher, Sara Sangtarash, Paul J. Low,* Wenjing Hong,* and Colin J. Lambert**

Abstract: *Together with the more intuitive and commonly recognized conductance mechanisms of charge-hopping and tunneling, quantum-interference (QI) phenomena have been identified as important factors affecting charge transport through molecules. Consequently, establishing simple and flexible molecular-design strategies to understand, control, and exploit QI in molecular junctions poses an exciting challenge. Here we demonstrate that destructive quantum interference (DQI) in meta-substituted phenylene ethylene-type oligomers (m-OPE) can be tuned by changing the position and conformation of methoxy (OMe) substituents at the central phenylene ring. These substituents play the role of molecular-scale taps, which can be switched on or off to control the current flow through a molecule. Our experimental results conclusively verify recently postulated magic-ratio and orbital-product rules, and highlight a novel chemical design strategy for tuning and gating DQI features to create single-molecule devices with desirable electronic functions.*

Introduction

Measurements of the conductance of electrode | molecule | electrode junctions, interpreted with the aid of theoretical treatments and computational modeling, have given insight into the fundamentals of through-molecule electron transport, leading to the design of molecular wires,[1] molecular switches,[2] and molecular diodes.[3] One of the most interesting aspects of single-molecule electronics to emerge from these studies is the phenomenon of room-temperature quantum interference (QI).[4] This concept was first introduced in 1909 to prove the wave characteristics of photons in the double-slit experiments.[5] Now it is widely investigated in diverse research areas, such as nanophotonics,[6] superconductivity,[7] and quantum metrology.[8] In the studies of molecular junctions, QI arises when the de Broglie waves of electrons progressing from one electrode to the other pass through different energetically accessible pathways across the molecule junction, causing interference patterns within the molecule.[9] Constructive QI (CQI) occurs when the interference pattern has a large amplitude at the point of molecular contact to both the source and drain electrodes, causing high through-molecule conductance. Conversely, destructive QI (DQI) results in a low amplitude of the propagating electron wave at one or both of the electrode–molecule contacts, causing extremely low through-molecule conductance.[10] The ability to convert between these two scenarios by tuning the molecular pathways can offer an exciting range of opportunities to regulate charge transport through molecules, without changing the molecular backbone structure, length, or redox state.

Recently, a number of studies have contributed to the identification of mechanisms for conductance tuning of single-molecule junctions using QI phenomena, including the impact of anchor groups,[11] the position of heteroatoms within the molecular backbone,[12] and bridge modification.[13] Following theoretical predictions of the introduction of DQI effects due to interactions of pendant oxygen and bipyridene groups with conjugated molecular cores[14] as well as subsequent experimental confirmation,[15] a study of QI effects in molecular junctions of π-conjugated systems was carried out by Guédon et al. using the conducting atomic force microscopy technique.[16] Arroyo et al. studied QI effects in a central phenyl ring by varying the coupling to a variety of anchor groups.[17] Manrique et al. have also demonstrated tuning of

[*] F. Jiang, H. Zheng, W. He, C. Zhu, C. Tang, R. Li, Dr. J. Liu, Prof. J. Shi, Prof. W. Hong
State Key Laboratory of Physical Chemistry of Solid Surfaces, College of Chemistry and Chemical Engineering, iChEM, Xiamen University
Xiamen 361005 (China)
E-mail: whong@xmu.edu.cn

D. I. Trupp, M. Korb, A. N. Sobolev, M. Naher, Prof. P. J. Low
School of Molecular Sciences, University of Western Australia
35 Stirling Highway, Crawley, Western Australia, 6009 (Australia)
E-mail: paul.low@uwa.edu.au

N. Algethami, Dr. A. Alqorashi, Dr. H. Sadeghi, Dr. S. Sangtarash, Prof. C. J. Lambert
Department of Physics, Lancaster University
Lancaster LA1 4YB (UK)
E-mail: c.lambert@lancaster.ac.uk

Dr. H. Sadeghi, Dr. S. Sangtarash
Present address: School of Engineering, University of Warwick, Coventry CV4 7AL (UK)
E-mail: s.sangtarash@lancaster.ac.uk

Dr. R. Davidson
Department of Chemistry, Durham University
Durham, DH1 3LE (UK)

Supporting information and the ORCID identification number(s) for the author(s) of this article can be found under: https://doi.org/10.1002/anie.201909461.

QI effects through heteroatom substitution within a molecular core, and proposed a quantum-circuit rule for designing molecular devices and materials.[18] Furthermore, the experimental and theoretical breakthroughs realized by Garner et al. have demonstrated that destructive QI effects are also achieved in silicon-based σ-orbital systems.[4a] More recently, Li et al. and Bails et al. have demonstrated control over through-molecule conductance by electrochemical gating of compounds displaying pronounced DQI anti-resonance features in their transmission profiles.[19] Although state-of-the-art theoretical studies have been devoted to the investigation of intramolecular QI patterns,[20] combined experimental and theoretical studies exploring the influence of both location and conformation of additional pendant groups on QI effects are missing. This study sets out to explore, both theoretically and experimentally, whether varying the locations and conformations of pendant groups at a molecular backbone could provide a new strategy for tuning QI effects and hence molecular conductance.

In this study, density functional theory (DFT) analysis (Supporting Information, Sections S1–S4) supported by experimental studies using the scanning tunneling microscope break-junction (STM-BJ) technique[21] (Figure 1 and Supporting Information, Sections S5–S7) have been used to investigate single-molecule charge transport through a series of *m*-

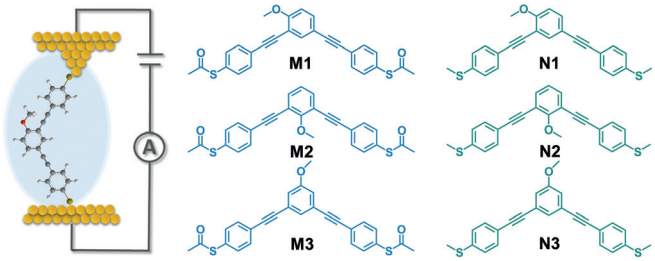

Figure 1. Schematic STM-BJ setup and structures of the molecules investigated in this work.

OPE molecules with thiolate (protected in the precursor as thioacetyl, SAc; **M1**–**3**) or thiomethyl (SMe; **N1**–**3**) anchor groups (Supporting Information, Sections S8 and S9). The results from these two families of compounds **M** and **N** with different anchor groups have been compared to ensure that the phenomena observed are due to the backbone and not some molecule–contact artifacts. The molecular *m*-OPE backbones are systematically modified by the introduction of a pendant OMe substituent at different positions around the central ring (Figure 1). The only difference between these molecules is the position and lowest-energy conformation of the pendant OMe group relative to the planar *meta*-diethynylphenylene core. For these molecular systems, DFT studies indicate that the OMe groups act as molecular "taps" which can be used to switch the current through the molecules on or off by modulating the QI signature. Figure 2a shows two conformations of the OMe tap of **M2** (modeled as the free thiol). The off-conformation (i) features the OMe group perpendicular to the plane of the molecule and corresponds to a low-conductance state for the *m*-OPE fragment that is

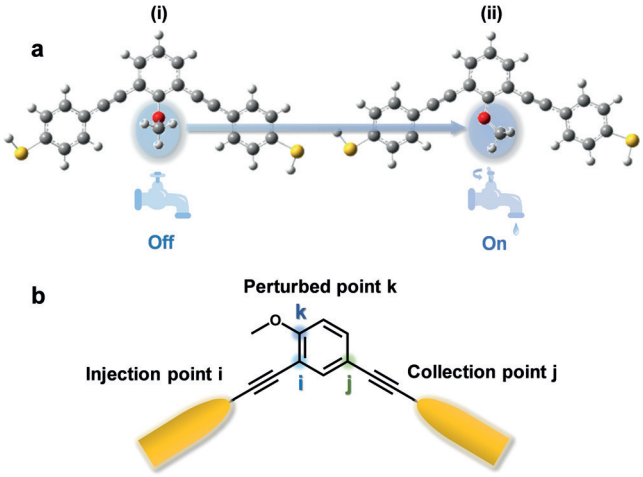

Figure 2. a) Two conformations of the molecular tap **M2** (shown as the free thiol). Rotating the OMe group from the off-conformation (i) to the on-conformation (ii) switches the *m*-OPE molecule from low to high conductance as the position of the DQI feature shifts. b) Conceptual view of the magic-ratio model of a molecular junction. The yellow regions represent compound electrodes which inject and collect electrons into the π-orbitals of the central ring via the triple bonds at points *i* and *j*, respectively. A perturbation associated with a pendant group is introduced at site *k*, illustrated schematically here for the substitution pattern of **M1**/**N1**.

similar to the parent system derived from 1,3-diethynylbenzene. Rotating the OMe group into the molecular plane gives the on-conformation (ii) and increases molecular conductance through the *m*-OPE moiety as the pendant oxygen becomes oriented to better serve as a π-donor and more effectively interfere with QI effects in the molecular π-system. These molecules have been designed so that the most energetically favorable conformation of the OMe tap in **M1** and **N1** is "on", whereas in the more sterically restricted **M2** and **N2**, it is "off". As discussed below, these molecules also demonstrate that the effectiveness of such molecular taps in controlling conductance is critically dependent on their connectivity to the central ring. Therefore, the location of the OMe taps in **M3** and **N3** has been chosen to render them completely ineffective, so that the electrical conductances of **M3** and **N3** are almost independent of the conformation of their pendant OMe groups.

The design of **M1**–**3** and **N1**–**3** is further informed by the recently described magic-ratio theory (Supporting Information, Section S2).[22] This theory describes the effect of connectivity on QI in the central aryl ring and views the moieties to the left and right as compound electrodes which inject and collect electrons via triple bonds into π-orbitals at points *i* and *j*, respectively (Figure 2b). The theory applies to the commonly encountered case where electrons tunnel through the HOMO–LUMO gap (that is, the Fermi energy of the electrodes lies within the molecular HOMO–LUMO gap; see Supporting Information, Section S3). For **M1**–**3** and **N1**–**3**, the injection and collection points *i* and *j* (Figure 2b) are in *meta* positions relative to each other, and as such, the bare parent molecule (with no OMe group) exhibits a DQI feature near the middle of the HOMO–LUMO gap and

possesses a low conductance.[9a] In a first approximation, if a perturbation to the parent structure is imposed on the central ring at a position *k*, for example, through the introduction of a pendant or substituent group, to yield a daughter molecule, then the magic-ratio theory predicts the following rules:[12]

1. If, as in **M1** and **N1**, *k* is *ortho* to *i* and *para* to *j*, then the pendant group will increase the conductance by shifting the DQI feature to a higher or lower energy.
2. If, as in **M2** and **N2**, *k* is *ortho* to both *i* and *j*, then the pendant group will increase the conductance by shifting the DQI feature in the opposite direction as in case 1.
3. If, as in **M3** and **N3**, *k* is *meta* to either *i* or *j*, then the pendant group will be ineffective and have only a small effect on the conductance. Consequently, the conductance of the daughter molecule remains low, as in the parent system.

The above changes in conductance are predicted to occur only if the pendant group perturbs the central ring by coupling to its π-system (Supporting Information, Section S2). When this happens, as for the lowest-energy conformation of **M1**/**N1** (which also conforms to the crystallographically determined structure of **N1**; Supporting Information, Section S9) or the (higher-energy) planar conformation of **M2**/**N2** (see Figure 2a-ii), the QI tap is turned on and the conductances of **M1**, **M2**, **N1**, and **N2** will be high. On the contrary, for the most energetically favorable conformation of **M2**/**N2**, where for steric reasons the OMe group rotates out of the molecular plane (see Figure 2a-i and the single-crystal X-ray structure of **N2** in the Supporting Information, Section S9), the non-bonding electron pair on the OMe oxygen atom is orthogonal to the π-system of the central ring. In this lower-energy orthogonal conformer, the OMe group does not significantly perturb the π system of the central ring and the tap is turned off. Consequently, the conductance of the *m*-OPE daughter molecules **M2**/**N2** is expected to remain low. Therefore, by computing and measuring the electrical conductances of **M1**–**3** and **N1**–**3**, the effect of both connectivity and conformation of the pendant group on QI effects and hence the flow of electricity through the *m*-OPE-derived molecules can be explored.

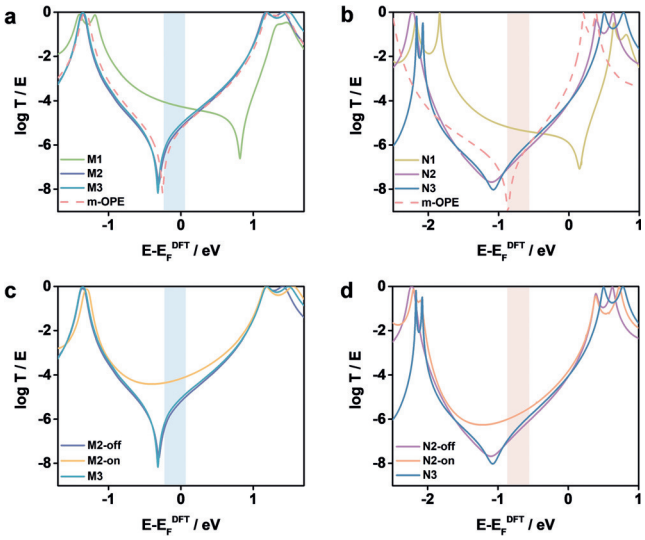

Figure 3. a), b) Transmission coefficients *T*(*E*) describing electrons of energy *E* passing through the *m*-OPE derivatives from one electrode to the other. In all cases, the dashed lines show results for the parent *m*-OPE. c) ,d) Transmission coefficients of the "off" and "on" **M2** (**N2**) molecule (see Figure 2a). For comparison, the transmission of the relaxed molecule **M3** (**N3**) is also shown.

Results and Discussion

To probe the role of the OMe groups, DFT calculations combined with the quantum-transport code Gollum[23] were used to compute the transmission coefficients of the systems. Plots of the transmission coefficients *T(E)* of *m*-OPE derivatives **M1**–**2** and **N1**–**3** in their fully relaxed geometries are shown in Figure 3a,b. The transmission function $T(E_F)$ evaluated at the Fermi energy E_F of the electrodes reflects the magnitude and trends of the electrical conductance *G* of the molecules. The experimental determination of molecular-orbital energies relative to E_F may differ from the DFT-predicted values. Typically, E_F is expected to lie in the vicinity of the middle of the HOMO–LUMO gap (Supporting Information, Section S3), and based on fitting to the experimentally determined conductance values (see below), the present results suggest that E_F falls within the shaded regions in Figure 3 (see Table 1).[24]

The conductance of the parent molecule *m*-OPE with thiolate contacts has been previously determined to be $10^{-5.5}$ G_0.[12b] Figure 3a shows that the transmission function of this parent *m*-OPE (dashed line) possesses a DQI dip near the middle of the HOMO–LUMO gap and that the function is almost matching that of **M3** (also contacted as the thiolate within the junction) over a wide range of energies, which demonstrates that the OMe tap is ineffective in this location. In contrast, the DQI dip of (deprotected) **M1** is shifted to higher energies and therefore, if the Fermi energy E_F in the experiment lies in the vicinity of E_F^{DFT}, the electrical conductance of **M1** is higher than that of **M3** (Figure 3a). These features are also observed in **N1** and **N3** (Figure 3b), and they are in agreement with rules 1 and 3 of the magic-ratio theory described above as well as the trends observed in related studies of the effect of substituent groups on QI.[12,20b] On the contrary, the DQI dip of (deprotected) **M2** in the fully relaxed

Table 1: Calculated and experimentally determined single-molecule conductances of **M1**–**3** and **N1**–**3**.

Molecule	Calc. log(G/G_0)	Exp. log(G/G_0)
M1	−4.25	−4.88
M2 (OMe on)	−4.18	
M2 (OMe off)	−5.24	−5.87
M3	−5.05	−5.55
N1	−5.35	−5.03
N2 (OMe on)	−5.56	
N2 (OMe off)	−6.26	−5.98
N3	−6.05	−5.74

(non-planar) geometry is not shifted and therefore, the electrical conductance of **M2** remains low. This result for **M2** is entirely consistent with the experimental data presented below (Table 1), but at first inspection, it seems to be contrary to the effect of the perturbation described by rule 2, which has been demonstrated to correctly predict the effect of substituents on QI in aryl rings.[12,20b] However, in these earlier studies, molecular conformation played no role. Here, the transmission coefficients of the off- and on-conformations of molecules **M2** (Figure 3c) and **N2** (Figure 3d) demonstrate a clear and significant conformational effect. While a rotation of the pendant group of **M2** or **N2** into the planar conformation removes the DQI dip from the middle of the HOMO–LUMO gap (Figures 3c,d and S1), this local minimum described by the planar geometry of the on-state is higher than that of the orthogonal conformation (+11.0 (**M2**), +12.7 kJ mol^{-1} (**N2**)). Therefore, the lower-energy off-conformations are favored and determine the conductance properties of the junctions.

The presence or absence of DQI transmission dips and the effect on mid-gap conductance can also be linked to the structure of the HOMO and LUMO through a recently highlighted orbital-product rule (Figure 4).[25] Even though these molecules do not possess particle–hole symmetry and therefore the orbital-symmetry rule[26] and the Coulson–Rushbrooke pairing theorem[27] do not apply, a qualitative indication of the presence or absence of DQI can be obtained by examining the interference between HOMO and LUMO. The rule is applied by noting that if the HOMO (LUMO) amplitudes of a molecule at the electrode contacts have the same sign, then the HOMO (LUMO) is assigned an orbital product a_H (a_L) which is positive. Conversely, if the HOMO (LUMO) amplitudes at the contacts have opposite sign, the orbital product a_H (a_L) will be negative. The orbital-product rule states that if a_H and a_L possess the same sign (that is, if the product $a_H{\cdot}a_L$ is positive), then the HOMO and LUMO interfere destructively and the transmission function is likely to possess a DQI dip. Otherwise, CQI occurs and there will be no dip. As indicated in Figure 4, the nodal properties and distributions of the HOMO and LUMO of **N2** in the lower-energy off-conformation are identical to those of the parent *m*-OPE because the π system of the OMe group is orthogonal to, and therefore decoupled from, the π-system of the central ring. Similar patterns are also found for **N3**, where the OMe group is located at a node in both the HOMO and LUMO. In each case, a_H and a_L are both negative, and the orbital-product rule predicts that **N2, N3**, and the parent molecule *m*-OPE will all exhibit DQI and possess low molecular conductances. In contrast, the opposing signs of a_H and a_L indicate that **N1** should exhibit CQI and possess a high conductance, in agreement with the observed conductance trends (the analogous trends and results from the **M**-series are shown in Table S6). Additionally, if the OMe tap of **N2** is artificially rotated to the on-position, as shown in the bottom row of Figure 4, the orbital product switches sign and CQI occurs.

To provide experimental support for the above predictions, the STM-BJ technique was employed to investigate the single-molecule conductance of all molecules in trimethylbenzene (TMB) at room temperature (Supporting Information, Section S5).[15a] Typical individual conductance–distance traces of the solvent, **M1–3** (which bind in the junction as the thiolate after spontaneous cleavage of the protecting group; Figures S8–S10), and **N1–3** are shown on a semi-logarithmic scale in Figure 5a,b.[28] The curves for the pure solvent (purple traces) exhibit the expected exponential decay after the cleavage of the last gold–gold atomic contact at the quantum conductance G_0 ($G_0 = 2e^2h^{-1}$),[29] while the traces for **M1–3** and **N1–3** show distinct molecular plateaus, indicating the formation of single-molecule junctions. Over 2000 conductance–distance traces were analyzed to produce the corresponding 1D histograms featuring distributions with clear peaks (Figure 5c,d). These 1D histograms were fitted by Gaussian functions, and the peaks of their distributions are attributed to the conductance of the most probable molecular configurations in the junction, that is, $10^{-4.88}$ G_0, $10^{-5.87}$ G_0, and $10^{-5.55}$ G_0 for **M1–3**, respectively, and $10^{-5.03}$ G_0, $10^{-5.98}$ G_0, and $10^{-5.74}$ G_0 for **N1–3**, respectively.

The displacement-distribution histograms and two-dimensional (2D) conductance–displacement histograms of **M1** and **N1** are shown in Figure 5e,f by way of example (for analogous data from the other molecules, see Figure S6).[30] Taking the data from **M1** as illustrative of the general analysis, the most probable length of the molecular junction is determined to be

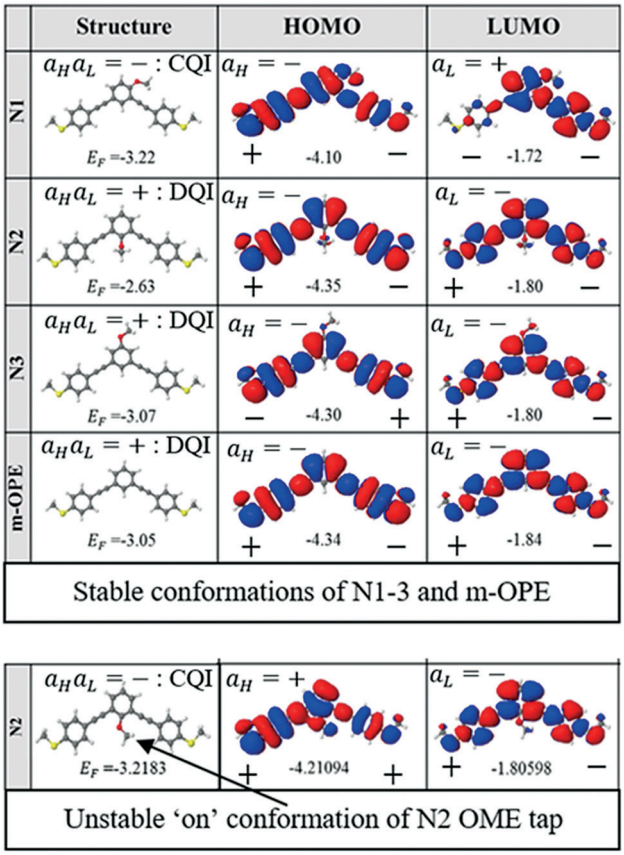

Figure 4. HOMOs and LUMOs of molecules **N1–N3** and the parent molecule *m*-OPE. Blue regions: positive sign, red regions: negative sign. As an example, for **N1**, the HOMO has a positive sign at the left end of the molecule and a negative sign at the right end. The orbital product a_H is therefore negative. Similarly, for **N1**, a_L is negative. Since the product of $a_H{\cdot}a_L$ is positive, **N1** will exhibit DQI.

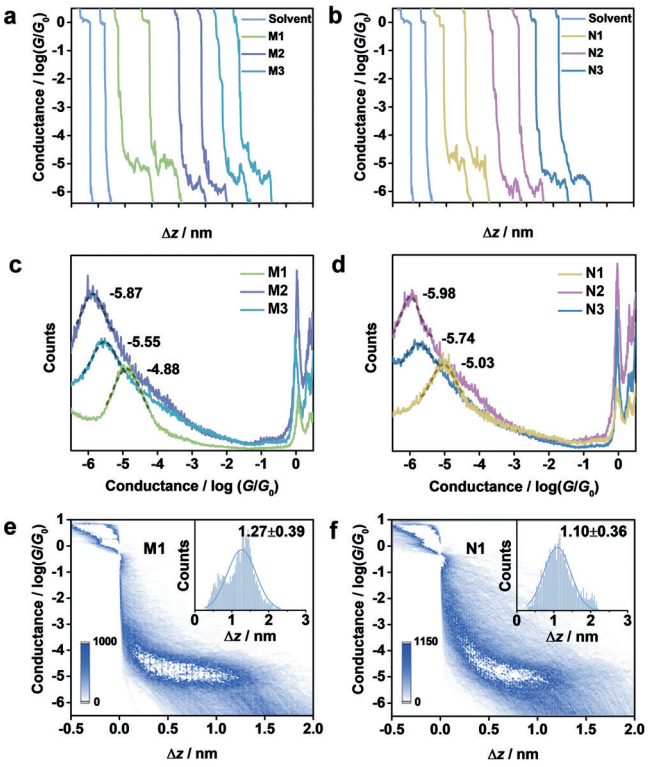

Figure 5. a), b) Typical individual conductance–distance traces of the pure solvent (TMB) and a) **M1**, **M2**, and **M3** as well as b) **N1**, **N2**, and **N3**. c), d) All-data-point 1D conductance histograms of c) **M1**, **M2**, and **M3** as well as d) **N1**, **N2**, and **N3** constructed from over 2000 traces for each histogram without data selection. e), f) Representative 2D conductance–displacement histogram and inset showing the displacement distribution of **M1** (e) and **N1** (f).

1.77 ± 0.39 nm after correcting for the snap-back effect of the gold–gold atomic contact (0.5 nm; Figure 5e and Supporting Information, Section S6).[15a] These measurements and computational estimates of the junction length are remarkably consistent with all the members of both series (Figure S6, Tables S3 and S4), suggesting that the molecules are in contact through the sulfur atoms in the molecular junctions. The histograms composed from **M2**/**N2** and **M3**/**N3** appear to capture a broader range of conductance features than those of **M1**/**N1** (Figure 5c,d and Table S7). These arise because the conductances of **M2**/**N2** and **M3**/**N3** are very close to the lower detection limit of the instrument used for the STM-BJ measurements (-7 to $-6.5\log(G/G_0)$), and external electromagnetic interference and mechanical vibration will have a more pronounced influence on these conductance data. In order to avoid the influence of the unstable molecular junctions on the measurements, 1D conductance histograms have also been reconstructed from data points only within the limited displacement range (0.9–1.1 nm), where the conductance plateaus are relatively flat and close to full extension (Figure S7). The conductance peaks and corresponding most probable conductance values from this limited data set are very similar to the results of the original full-range 1D conductance histograms, suggesting that the unstable junctions or lower yields of junctions might affect the shapes and distributions of 1D conductance histograms but not distinctly change the conductance values.

To exclude the influence of physisorbed sulfur contacts and the formation of junctions retaining the acetyl-protecting groups,[31] single-molecule measurements of the **M**-series of molecules were also recorded after adding 3 equiv of Bu_4NOH to the sample solution to ensure the cleavage of the acetyl moiety. The resulting conductance–distance traces and conductance histograms were consistent with those of the junctions formed from the same molecules by spontaneous cleavage of the protecting group in the pristine solvent (Figure S8–S10).[31,32] To rule out further possibilities of intramolecular π–π stacking effects within the junction[33] or coincidental electrode contacts to the methoxy moiety,[34] two model tolane compounds, 4-((4-methoxyphenyl)ethynyl)-phenyl (methyl)sulfane (**O1**) and 4-((3-methoxyphenyl)ethynyl)phenyl (methyl)sulfane (**O2**), were also measured (Figure S11). Under conditions identical to those used in the studies of **M1**–**3** and **N1**–**3**, no clear molecular plateaus were observed in the conductance histograms of **O1** and **O2**. These control experiments, together with the excellent agreement of the break-off distance and the molecular length of **M1**–**3** and **N1**–**3**, give us confidence that the single-molecule conductance features illustrated in Figure 5 can be attributed to single-molecule junctions formed by contact of the gold electrodes to the two sulfur-atom anchors of **M1**–**3** and **N1**–**3**.

The conductance values (G) within each series follow a pronounced pattern of variation, with G(**M1**/**N1**) > G(**M3**/**N3**) > G(**M2**/**N2**). This pattern is entirely consistent with the broad predictions of the magic-ratio theory described above combined with the DFT predictions for the conformation of the OMe group relative to the central phenylene ring, which determines the on–off nature of the OMe tap.

Conclusion

In conclusion, we have investigated the possibility of tuning DQI within *m*-OPE-derived molecules by placing OMe taps at different positions at the central ring. Our combined DFT predictions and STM-BJ measurements demonstrate that the position and orientation of the OMe taps have a significant impact on the energy of the DQI-induced dips in the transmission function. As a consequence of this DQI tuning, the conductance of **M1**/**N1** is almost one order of magnitude higher than that of the parent system *m*-OPE, whereas the conductances of **M3**/**N3** remain low. On the contrary, the influence of the OMe group on the mid-gap DQI feature also strongly depends on the on–off conformation of the OMe tap. This is illustrated by **M2**/**N2,** whose most energetically favorable conformation is "off" and corresponds to weak coupling between the pendant group and the molecular core. This work presents a simple and convenient approach for structurally tuning room-temperature DQI at a single-molecule level and demonstrates a new strategy for designing molecular devices with enhanced switching functionality.

Experimental Section

CCDC 1876564 and 1876565 contain the supplementary crystallographic data for this paper. These data can be obtained free of charge from The Cambridge Crystallographic Data Centre.

Acknowledgements

This work was supported by the National Key R&D Program of China (2017YFA0204902), National Natural Science Foundation of China (Nos. 21673195, 21703188, 21503179). It was also supported by EPSRC grants EP/P027156/1, EP/N03337X/1, EP/N017188/1, the EC H2020 FET Open project 767187 "QuIET", the EU project Bac-to-Fuel, and the Australian Research Council (DP190100074). S.S. thanks the Leverhulme Trust (Leverhulme Early Career Fellowships no. ECF-2018-375) for funding. H.S. acknowledges the UKRI Future Leaders Fellowship no. MR/S015329/1. M.N. and M.K. gratefully acknowledge support from the Forrest Research Foundation. The crystallographic structures of **N1** and **N2** were determined using facilities and instrumentation provided by the Centre for Microscopy, Characterisation and Analysis (CMCA), University of Western Australia.

Conflict of interest

The authors declare no conflict of interest.

Keywords: density functional calculations · destructive quantum interference · scanning tunnelling microscope break junction · single-molecule studies

How to cite: *Angew. Chem. Int. Ed.* **2019**, *58*, 18987 – 18993
Angew. Chem. **2019**, *131*, 19163 – 19169

[1] a) N. Algethami, H. Sadeghi, S. Sangtarash, C. J. Lambert, *Nano Lett.* **2018**, *18*, 4482 – 4486; b) W. Xu, E. Leary, S. Hou, S. Sangtarash, M. T. González, G. Rubio-Bollinger, Q. Wu, H. Sadeghi, L. Tejerina, K. E. Christensen, N. Agraït, S. J. Higgins, C. J. Lambert, R. J. Nichols, H. L. Anderson, *Angew. Chem. Int. Ed.* **2019**, *58*, 8378 – 8382; *Angew. Chem.* **2019**, *131*, 8466 – 8470.

[2] a) C. D. Frisbie, *Science* **2016**, *352*, 1394 – 1395; b) F. Chen, J. He, C. Nuckolls, T. Roberts, J. E. Klare, S. Lindsay, *Nano Lett.* **2005**, *5*, 503 – 506; c) T. A. Su, H. Li, M. L. Steigerwald, L. Venkataraman, C. Nuckolls, *Nat. Chem.* **2015**, *7*, 215 – 220.

[3] a) X. Chen, M. Roemer, Y. Li, D. Wei, D. Thompson, E. D. Barco, C. A. Nijhuis, *Nat. Nanotechnol.* **2017**, *12*, 797 – 803; b) I. Díez-Pérez, J. Hihath, Y. Lee, L. Yu, L. Adamska, M. A. Kozhushner, I. I. Oleynik, N. Tao, *Nat. Chem.* **2009**, *1*, 635 – 641.

[4] a) M. H. Garner, H. Li, Y. Chen, T. A. Su, Z. Shangguan, D. W. Paley, T. Liu, F. Ng, H. Li, S. Xiao, C. Nuckolls, L. Venkataraman, G. C. Solomon, *Nature* **2018**, *558*, 415 – 419; b) R. Frisenda, V. A. E. C. Janssen, F. C. Grozema, H. S. J. van der Zant, N. Renaud, *Nat. Chem.* **2016**, *8*, 1099 – 1104.

[5] G. I. Taylor, *Proc. Cambridge Philos. Soc.* **1909**, *15*, 114 – 115.

[6] a) N. C. Harris, G. R. Steinbrecher, M. Prabhu, Y. Lahini, J. Mower, D. Bunandar, C. Chen, F. N. C. Wong, T. Baehr-Jones, M. Hochberg, S. Lloyd, D. Englund, *Nat. Photonics* **2017**, *11*, 447 – 453; b) A. Sipahigil, R. E. Evans, D. D. Sukachev, M. J. Burek, J. Borregaard, M. K. Bhaskar, C. T. Nguyen, J. L. Pacheco, H. A. Atikian, C. Meuwly, R. M. Camacho, F. Jelezko, E. Bielejec, H. Park, M. Lončar, M. D. Lukin, *Science* **2016**, *354*, 847 – 850.

[7] a) C. Schuck, X. Guo, L. Fan, X. Ma, M. Poot, H. X. Tang, *Nat. Commun.* **2016**, *7*, 10352; b) S. Goswami, E. Mulazimoglu, A. M. R. V. L. Monteiro, R. Wölbing, D. Koelle, R. Kleiner, Y. M. Blanter, L. M. K. Vandersypen, A. D. Caviglia, *Nat. Nanotechnol.* **2016**, *11*, 861 – 865.

[8] Z.-E. Su, Y. Li, P. P. Rohde, H.-L. Huang, X.-L. Wang, L. Li, N.-L. Liu, J. P. Dowling, C.-Y. Lu, J.-W. Pan, *Phys. Rev. Lett.* **2017**, *119*, 080502.

[9] a) C. Lambert, *Chem. Soc. Rev.* **2015**, *44*, 875 – 888; b) D. Xiang, X. Wang, C. Jia, T. Lee, X. Guo, *Chem. Rev.* **2016**, *116*, 4318 – 4440.

[10] Y. Zhang, G. Ye, S. Soni, X. Qiu, T. L. Krijger, H. T. Jonkman, M. Carlotti, E. Sauter, M. Zharnikov, R. C. Chiechi, *Chem. Sci.* **2018**, *9*, 4414 – 4440.

[11] M. Kiguchi, T. Ohto, S. Fujii, K. Sugiyasu, S. Nakajima, M. Takeuchi, H. Nakamura, *J. Am. Chem. Soc.* **2014**, *136*, 7327 – 7332.

[12] a) S. Sangtarash, H. Sadeghi, C. J. Lambert, *Phys. Chem. Chem. Phys.* **2018**, *20*, 9630 – 9637; b) X. Liu, S. Sangtarash, D. Reber, D. Zhang, H. Sadeghi, J. Shi, Z. Y. Xiao, W. Hong, C. J. Lambert, S. X. Liu, *Angew. Chem. Int. Ed.* **2017**, *56*, 173 – 176; *Angew. Chem.* **2017**, *129*, 179 – 182.

[13] X.-F. Li, Q. Qiu, Y. Luo, *J. Appl. Phys.* **2014**, *116*, 013701.

[14] a) T. Papadopoulos, I. Grace, C. Lambert, *Phys. Rev. B* **2006**, *74*, 193306; b) C. Finch, V. Garcia-Suarez, C. Lambert, *Phys. Rev. B* **2009**, *79*, 033405.

[15] a) W. Hong, H. Valkenier, G. Mészáros, D. Z. Manrique, A. Mishchenko, A. Putz, P. M. García, C. J. Lambert, J. C. Hummelen, T. Wandlowski, *Beilstein J. Nanotechnol.* **2011**, *2*, 699 – 713; b) V. Kaliginedi, P. Moreno-García, H. Valkenier, W. Hong, V. M. García-Suárez, P. Buiter, J. L. Otten, J. C. Hummelen, C. J. Lambert, T. Wandlowski, *J. Am. Chem. Soc.* **2012**, *134*, 5262 – 5275.

[16] a) C. M. Guédon, H. Valkenier, T. Markussen, K. S. Thygesen, J. C. Hummelen, S. J. Van Der Molen, *Nat. Nanotechnol.* **2012**, *7*, 305 – 309; b) D. Z. Manrique, Q. Al-Galiby, W. Hong, C. J. Lambert, *Nano Lett.* **2016**, *16*, 1308 – 1316.

[17] C. R. Arroyo, S. Tarkuc, R. Frisenda, J. S. Seldenthuis, C. H. Woerde, R. Eelkema, F. C. Grozema, H. S. Van Der Zant, *Angew. Chem. Int. Ed.* **2013**, *52*, 3152 – 3155; *Angew. Chem.* **2013**, *125*, 3234 – 3237.

[18] D. Z. Manrique, C. Huang, M. Baghernejad, X. Zhao, O. A. Al-Owaedi, H. Sadeghi, V. Kaliginedi, W. Hong, M. Gulcur, T. Wandlowski, *Nat. Commun.* **2015**, *6*, 6389.

[19] a) Y. Li, M. Buerkle, G. Li, A. Rostamian, H. Wang, Z. Wang, D. R. Bowler, T. Miyazaki, L. Xiang, Y. Asai, G. Zhou, N. Tao, *Nat. Mater.* **2019**, *18*, 357 – 363; b) J. Bailis, A. Daaoub, S. Sangtarash, X. Li, Y. Tang, Q. Zou, H. Sadeghi, S. Liu, X. Huang, Z. Tan, J. Liu, Y. Yang, J. Shi, G. Mészáros, W. Chen, C. Lambert, W. Hong, *Nat. Mater.* **2019**, *18*, 364 – 369.

[20] a) A. Danilov, S. Kubatkin, S. Kafanov, P. Hedegård, N. Stuhrhansen, K. Mothpoulsen, T. Bjørnholm, *Nano Lett.* **2008**, *8*, 1 – 5; b) M. H. Garner, G. C. Solomon, M. Strange, *J. Phys. Chem. C* **2016**, *120*, 9097 – 9103; c) G. C. Solomon, D. Q. Andrews, R. H. Goldsmith, T. Hansen, M. R. Wasielewski, R. P. Van Duyne, M. A. Ratner, *J. Am. Chem. Soc.* **2008**, *130*, 17301 – 17308.

[21] B. Xu, N. J. Tao, *Science* **2003**, *301*, 1221 – 1223.

[22] S. Sangtarash, H. Sadeghi, C. J. Lambert, *Nanoscale* **2016**, *8*, 13199 – 13205.

[23] J. Ferrer, C. J. Lambert, V. M. García-Suárez, D. Z. Manrique, D. Visontai, L. Oroszlany, R. Rodríguez-Ferradás, I. Grace, S. Bailey, K. Gillemot, *New J. Phys.* **2014**, *16*, 093029.
[24] a) H. Song, Y. Kim, Y. H. Jang, H. Jeong, M. A. Reed, T. Lee, *Nature* **2009**, *462*, 1039 – 1043; b) P. Moreno-García, M. Gulcur, D. Z. Manrique, T. Pope, W. Hong, V. Kaliginedi, C. Huang, A. S. Batsanov, M. R. Bryce, C. Lambert, *J. Am. Chem. Soc.* **2013**, *135*, 12228 – 12240.
[25] C. J. Lambert, S. X. Liu, *Chem. Eur. J.* **2018**, *24*, 4193 – 4201.
[26] a) K. Yoshizawa, T. Tada, A. Staykov, *J. Am. Chem. Soc.* **2008**, *130*, 9406 – 9413; b) X. Li, A. Staykov, K. Yoshizawa, *J. Phys. Chem. C* **2010**, *114*, 9997 – 10003; c) Y. Tsuji, A. Staykov, K. Yoshizawa, *J. Am. Chem. Soc.* **2011**, *133*, 5955 – 5965.
[27] C. Coulson, G. Rushbrooke, *Math. Proc. Cambridge Philos. Soc.* **1940**, *36*, 193 – 200.
[28] W. Hong, D. Z. Manrique, P. Moreno-García, M. Gulcur, A. Mishchenko, C. J. Lambert, M. R. Bryce, T. Wandlowski, *J. Am. Chem. Soc.* **2012**, *134*, 2292 – 2304.
[29] R. Huber, M. T. González, S. Wu, M. Langer, S. Grunder, V. Horhoiu, M. Mayor, M. R. Bryce, C. Wang, R. Jitchati, C. Schönenberger, M. Calame, *J. Am. Chem. Soc.* **2008**, *130*, 1080 – 1084.
[30] D. Z. Manrique, C. Huang, M. Baghernejad, X. Zhao, O. A. Al-Owaedi, H. Sadeghi, V. Kaliginedi, W. Hong, M. Gulcur, T. Wandlowski, M. R. Bryce, C. J. Lambert, *Nat. Commun.* **2015**, *6*, 6389.
[31] M. T. GonzáLez, E. Leary, R. Garcia, P. Verma, M. A. N. Herranz, G. Rubio-Bollinger, N. Martin, N. Agrait, *J. Phys. Chem. C* **2011**, *115*, 17973 – 17978.
[32] V. Hennie, E. H. Huisman, P. A. van Hal, D. M. de Leeuw, R. C. Chiechi, J. C. Hummelen, *J. Am. Chem. Soc.* **2011**, *133*, 4930 – 4939.
[33] S. Martín, I. Grace, M. R. Bryce, C. Wang, R. Jitchati, A. S. Batsanov, S. J. Higgins, C. J. Lambert, R. J. Nichols, *J. Am. Chem. Soc.* **2010**, *132*, 9157 – 9164.
[34] O. A. Al-Owaedi, S. Bock, D. C. Milan, M.-C. Oerthel, M. S. Inkpen, D. S. Yufit, A. N. Sobolev, N. J. Long, T. Albrecht, S. J. Higgins, *Nanoscale* **2017**, *9*, 9902 – 9912.

Manuscript received: July 27, 2019
Revised manuscript received: September 30, 2019
Accepted manuscript online: October 15, 2019
Version of record online: October 31, 2019

